Light Metals 2012 *Edited by: Carlos E. Suarez*
TMS (The Minerals, Metals & Materials Society), 2012

THE EFFECT OF FRICTION STIR WELDING ON THE MICROSTRUCTURE AND TENSILE PROPERTIES OF AL 2139-T8 ALLOYS

Tomoko Sano[1], Jian Yu[1], Jessica Medintz[2] Chian-Fong Yen[1], Kevin Doherty[3]
[1]U.S. Army Research Laboratory, RDRL-WMM-B, Aberdeen Proving Ground, MD 21005 USA
[2]University of Texas at San Antonio, One UTSA Circle, San Antonio, TX 78249
[3]U.S. Army Research Laboratory, RDRL-WMM-F, Aberdeen Proving Ground, MD 21005 USA

Keywords: Al 2139, Friction Stir Weld, Tensile Properties

Abstract

The welding process introduces heat, plastic deformation, and chemical variation into the weld joints and alters the microstructure, strength, and ductility of the welded region. In this research, two plates of Al 2139-T8 alloys were welded together by friction stir welding (FSW). An evaluation of the crystallographic texture, grain size, and morphology of the grains in the FSW region, in comparison to those of the grains outside of the weld region, was made by scanning electron microscopy (SEM) and electron backscattered diffraction. In addition, the quasi-static tensile behavior of samples from the FSW region and those from outside of the FSW region was characterized by in-situ tensile experiments in the SEM with digital image correlation. It was found that the ultimate tensile strength was greater in the samples from outside FSW region and the elongation was greater for samples from the FSW region. The full results of the effect of the FSW on the Al2139 microstructure and tensile behavior will be discussed in detail.

Introduction

Aluminum has become more desirable as replacement for steel in structural and vehicular components for the Army. Especially in protection systems, weight reduction must be conducted without sacrificing strength or performance. Such critical design factors must also apply to the joints, where aluminum plates meet. Compared to conventional welding techniques, friction stir welding (FSW) [1, 2] was found to be a better technique for joining aluminum parts [3]. FSW technique uses a welding tool with a rotating pin attached to a wider "shoulder" (See Fig. 1). The pin is inserted into the material and joins the parts together with heat generated from friction, the mechanical rotation, and adiabatic heat. The welding process creates the stir zone (SZ) thermal-mechanically affected zone (TMAZ), and the heat affected zone (HAZ), and causes severe plastic deformation and dynamic recrystallization (see Fig. 2). This results in a varying microstructure and mechanical properties, as a function of the distance away from the weld center [4, 5, 6]. To better understand the microstructural and mechanical property variations due to the welding process, characterization of the microstructure and tensile properties need to be conducted in the weld area and compare to those of the parent material, or unaffected areas outside of the weld.

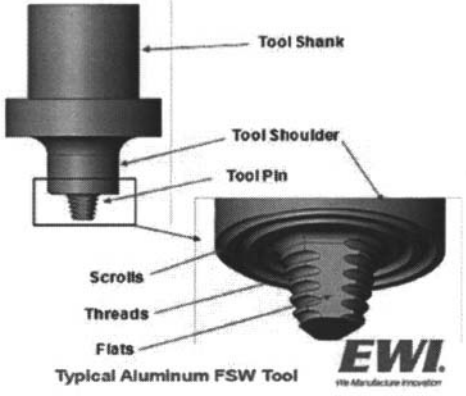

Figure 1. Friction Stir Weld tool

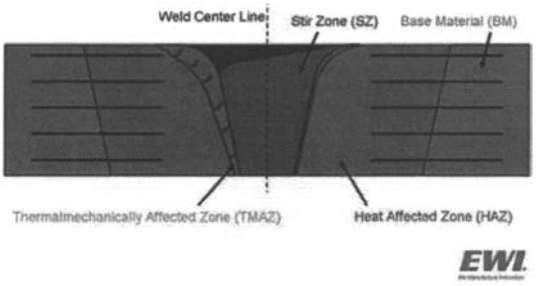

Figure 2. Schematic cross section of a FSW, indicating the stir zone, thermal-mechanically affected zone, and heat affected zone.

Experimental Procedures

Two Al 2139-T8 plates were welded together at EWI in Columbus, OH, using a tool with pin and shoulder features similar to the one shown in figure 1. The FSW parameters used are tabulated in Table I. Using electric discharge machining, tensile specimens with a gauge length of 15 mm, width of 2 mm, and thickness of 0.8 mm were cut out of the plate surface, and specimens with a gauge length of 8 mm, width of 2 mm and thickness of 0.8 mm were cut from the through thickness of the plate. A set of samples oriented in the X, Y, and Z directions were obtained from the FSW SZ and also from the base material, outside of the weld section (see Fig. 3). The samples were polished using the Struers RotoPol-31 polisher, starting with 600 grit SiC, then 9 micron diamond solution, and with diamond solutions of incrementally decreasing particle size on polishing cloth until reaching the 1 micron particle size. Further polishing

Table I Friction stir welding parameters

Parameter	Specification
Shoulder Diameter	1.625"
Pin Length	0.972"
Plunge Depth	0.02-0.005"
Spindle Speed	150-250 RPM
Travel Speed	2 IPM
Total Length	18"

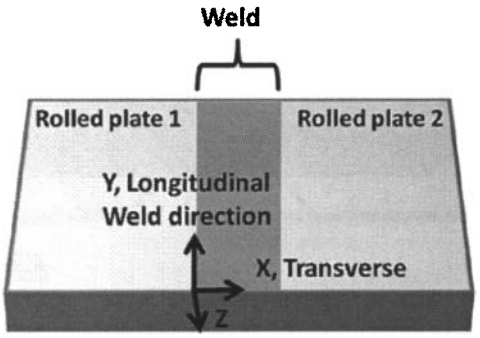

Figure 3. Schematic of the two welded plates and the sample directions

with 0.04 micron colloidal silica on final polishing cloth was performed for samples to be examined by the scanning electron microscope (SEM) and electron backscattered diffraction (EBSD).

The FEI Nova NanoSEM 600 SEM was used to characterize the microstructure before the tensile tests. EBSD characterization of the crystallographic orientation texturing of the samples were conducted at 20 kV accelerating voltage, spot size of 5, and at 70° tilt with the EDAX/TSL EBSD system in the SEM. EBSD patterns were collected from the gauge section of each tensile sample. The collected data was minimally "cleaned" by using the TSL OIM Analysis 5 "cleanup" program to correct incorrectly indexed points based on neighboring point's orientation correlation.

The Ernest Fullam in-situ tension and compression stage for the SEM coupled with the ADMET's MTEST Quattro™ interface and application program was used for some of the tension experiments. Strain rates on the order of 10^{-4} s^{-1} were applied to all samples. To validate the results of the in-situ tests, tensile tests were also performed on a screw driven Instron 1125 with a 1000 pound load cell, at the same strain rates as the in-situ tests. Load (N), displacement (mm), and time (s) were all measured and recorded by the Instron during testing.

To determine a more accurate modulus of elasticity, digital image correction (DIC) technique was applied for both testing techniques. For the in-situ tests, during the elastic regime, a series of SEM images of the microstructure were captured and corresponding live loads and positions were recorded. The image size was 1024 × 943 pixels; the field of view was about 16 mm^2. For the Instron tests, photos were taken every 15 seconds using a Nikon D300 camera with a 70 mm lens. The TIFF images were imported into GOM mbH's ARAMIS, a photogrammetric software, for strain analysis. The analysis procedure for ARAMIS was detailed in earlier report [7]. Here we used the 2-dimensional analysis procedure, in which only one camera view was required. The optimal facet size is 51 × 51 pixels and the optimal facet step overlap is 25 pixels. A signal filter was applied to remove noise (2 × 7 filter runs; replacing the facet point value with the median value among the 49 neighboring facet points and itself). In addition to the local strain contour plots, three virtual digital strain gauges were placed on the specimen surface to obtain the average bulk strain. The average bulk strain and load values were used to plot more accurate stress strain curves to calculate the elastic modulus.

Results

Crystallographic orientation data were collected with the EBSD on samples of all directions. The microstructures of the grains oriented in the X direction and in the Y direction were similar at the surface of the welded area. Samples from both X and Y directions showed comparable texture and grain size distributions. Figure 4(a) shows the color coded orientations in a standard stereographic triangle, and figure 4(b) the inverse pole figure (IPF) map of the scan area. The average grain size determined from a 2.2 mm^2 area was 14.0 μm with a standard deviation of 6.6 μm for the grains from the X direction sample and 18.1 μm with a standard deviation of 6.5 μm for those of the Y direction sample. The grains in the Z direction samples from the middle of the 1 inch thick plate showed evidence of recrystallization. The grains had a more random texture and a coarser, elongated shape, as shown in figure 5. The average grain size of these grains was 131.9 μm, with a standard deviation of 83.9 μm. This indicates significant anisotropy in the weld area along the through thickness. To quantify the texture differences between the grains in the plate surface and those in the through

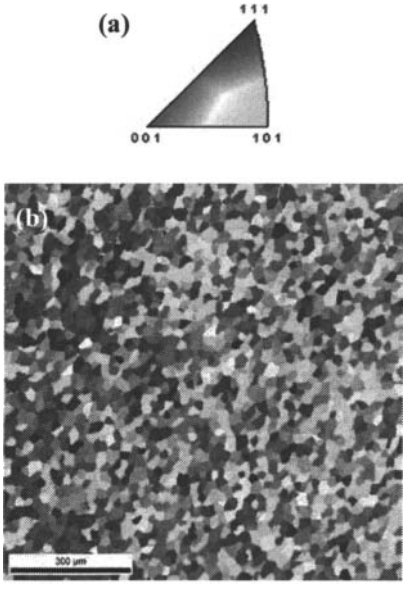

Figure 4. (a) IPF map color key and (b) IPF map of a Y direction sample from the weld area

thickness, the IPF texture plot of the grains in figure 3 and grains from numerous EBSD scans of the Z direction sample were plotted. The IPF texture plot of the grains in the X and Y direction sample showed a strong preference to the [111] orientation (see

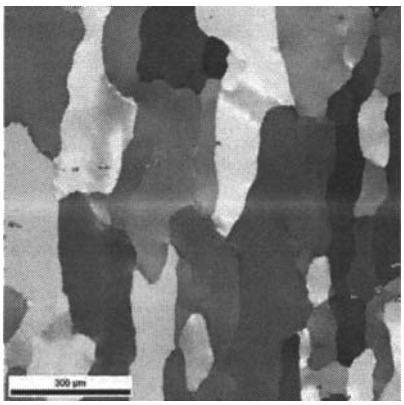

Figure 5. IPF map of a Z direction sample from the weld area

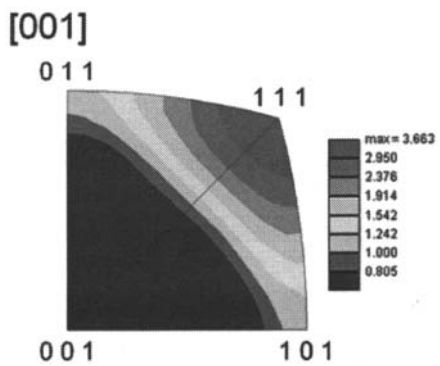

Figure 6. IPF texture plot of Y direction grains in the weld area determined from grains in Fig. 3.

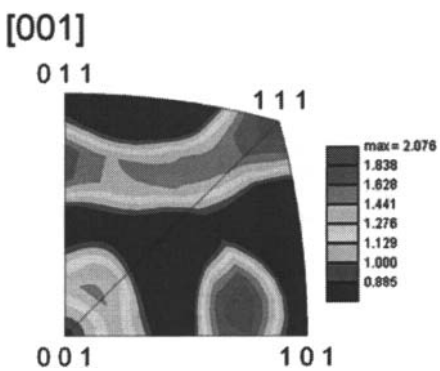

Figure 7. IPF texture plot of Z direction grains in the weld area determined from over 90 grains

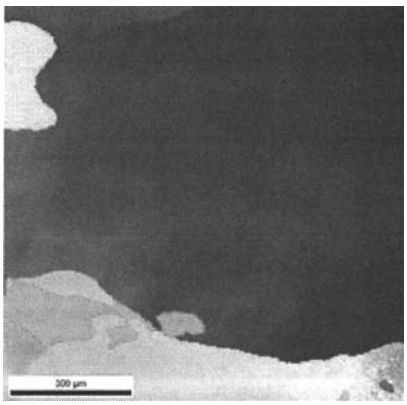

Figure 8. IPF map of a X direction sample from outside the weld area

Fig. 6) but the grains in the Z direction sample showed less texture and other preferred orientations, as shown in figure 7.

Outside the weld area, the grains were significantly larger, as indicated in figure 8. Not enough sampling was possible for a statistically significant texture and grain size analysis.

The tensile tests showed a different tensile behavior based on the sample location. Samples from the weld area had comparable ultimate tensile strength (UTS) and elongation, however the samples from outside of the friction stir weld area had higher strength but less ductility (see Fig. 9). Figure 10 shows the stress-strain curves of the X direction samples in the weld area and outside the weld area for the in-situ tests and the Instron tests. The results showed comparable ultimate tensile strength between the two testing techniques. However the initial slope of the curve varied, as did the elastic modulus. This difference was attributed to the in-situ tester possibly having grip slippage issues. Hence the elastic modulus values, shown in Table II, were determined from the Instron results. In addition to the Z direction samples having a lower elastic modulus, the UTS results (see Table II) also show a similar trend. The through thickness had lower UTS, regardless of whether the sample was from the weld area or outside the weld area.

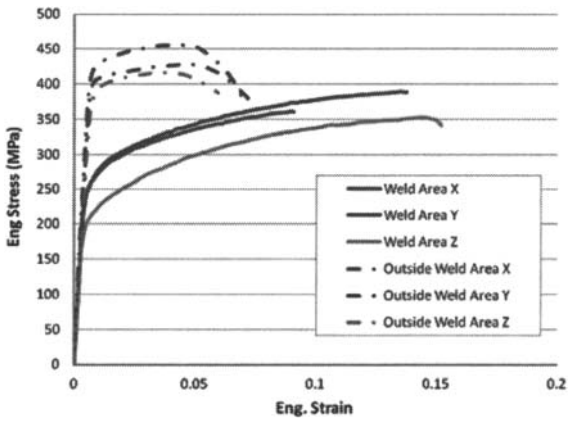

Fiigure 9. Instron stress-strain results of samples in the X, Y, and Z directions, inside the weld and outside the weld area.

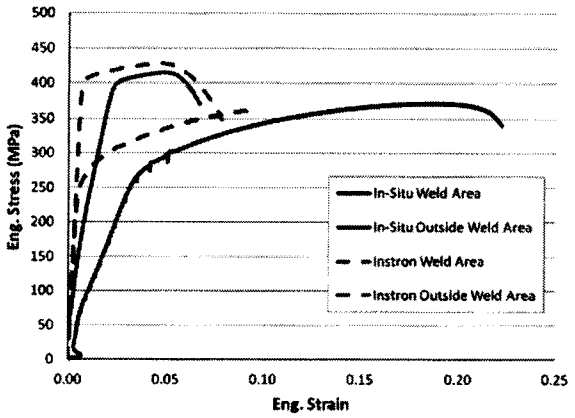

Figure 10. Comparison of the stress-strain curves from the Instron and In-Situ technique for the X direction in the weld area and outside the weld area.

Table II. Average Elastic Modulus and Average UTS of the weld area and outside of the weld area

	X	Y	Z
Modulus (GPa)	62.9 ± 6.4	63.6 ± 5.4	53.1 ± 3.8
Weld Area UTS (MPa)	362	389	353
Outside Weld Area UTS (MPa)	445	447	418

The fracture behavior differed based on the location of the sample with respect to the weld area. Figure 11 (a) is a SEM micrograph of the two fractured surfaces of the tensile sample in the Y direction, from the weld area. The fractured surface shows both brittle and ductile behavior with microcracks along grain boundaries and ductile failure by microvoid coalescence. Other researchers have observed microcracking in in-situ tests on aluminum [8]. The fractured edge of the Z direction samples in the weld area showed what looked to be brittle transgranular fracture (see Fig. 11 (b)). However the fractured surfaces still showed microvoid coalescence. The microvoids, however were on the order of 0.3 μm in diameter, compared to 1.4 μm for those in the Y direction sample. Although showing both brittle and ductile failure modes, a comparison of the Y direction and Z direction micrographs, shows that there are anisotropic effects in the failures. Outside the weld area, there was no evidence of brittle failure. Slip bands, void nucleation and particle interface decohesion was apparent, as shown in figure 11 (c).

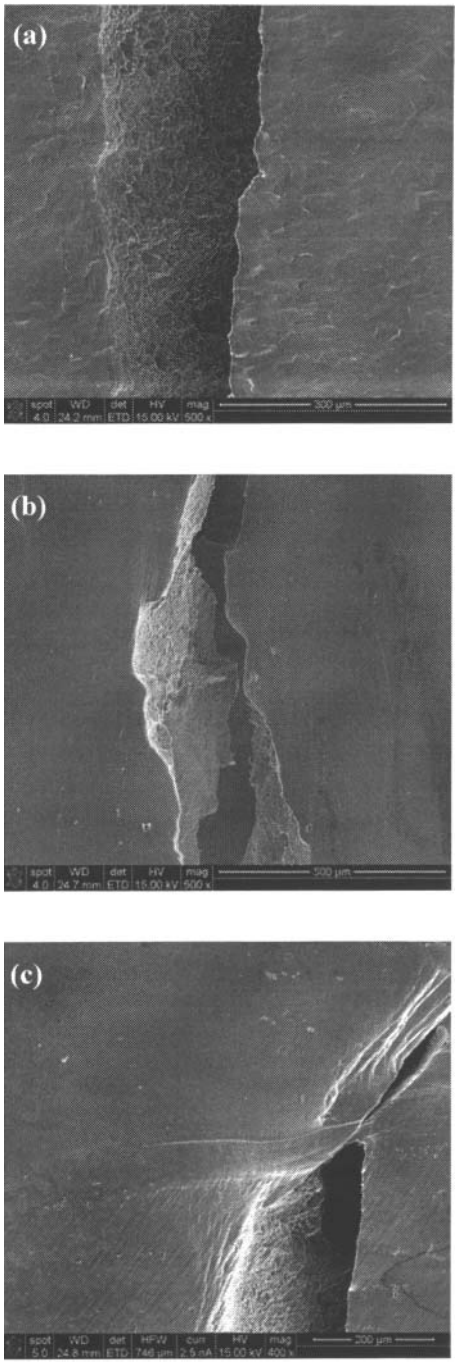

Figure 11 (a) Fractured surface of the Y direction sample in the weld area, (b), the fractured surfaces of the Z direction in the weld area, and (c), fractured surfaces of the X direction sample outside of the weld area.

Discussion

The FSW process causes anisotropic microstructural zones, SZ, TMAZ, HAZ to form. In addition, in the SZ, grains undergo inhomogeneous plastic deformation, with varying degrees of dislocation densities, dynamic recrystallization, and recovery. This was supported by the larger grain size shown in figure 4 and more random crystal orientation shown in figure 8. All these variations in the grain morphology aspects within SZ produces a mismatch in stresses, reducing the UTS and elastic modulus for the Z direction sample from the weld area. The increase in ductility of the samples in the weld area compared to the samples outside of the weld is due to the improvement in the work hardening rate from the increase in dislocations.

Conclusions

Two Al 2139-T8 plates were joined together by FSW. Tensile tests were conducted with both in-situ tensile stage in the SEM and with the Instron 1125 system. Comparable UTS and elongation results were observed with the two testing systems. Comparison of the microstructure and tensile behavior between samples from the weld area and outside the weld area showed distinct differences. In addition, the differences in the texture, grain size, UTS, and elastic modulus between the X and Y planar direction samples in the weld and the through thickness Z direction sample in the weld was caused by the varying plastic deformation, recrystallization, and recovery in the SZ.

References

1. W. M. Thomas, E. D. Nicholas, J. C. Needham, M.G. Murch, P. Temple-Smith, J. C. Dawes, *Friction Stir Butt Welding. Patent Application Number 5,460,317* United States of America, 1995.

2. O. T. Midling, *Friction Stir Welding. 5813592* United States, September 29, 1998.

3. M. W. Mahoney, C. G. Rhodes, J. G. Flintoff, R. A. Spurling, and W. H. Bingel, "Properties of Friction-Stir-Welded 7075 T651 Aluminum," *Metallurgical and Materials Transactions A,* 29A, (1998), 1955-1964.

4. T. Hirata, T. Oguri, and H. Hagino, T. Tanaka, S. W. Chung, Y. Takigawa, and K. Higashi, "Influence of Friction Stir Welding Parameters on Grain Size and Formability in 5083 Aluminum," *Material Science & Engineering A*, 456, (2007) 344-349.

5. M. A. Sutton, B. Yang, A. P. Reynolds, R. Taylor, Microstructural Studies of Friction Stir Welds in 2024-T3 Aluminum," *Materials Science and Engineering A*, 323, (2002), 160-166.

6. A. Sullivan and J. D. Robson, "Microstructural Properties of Friction Stir Welded and Post-Weld Heat-Treated 7449 Aluminium Alloy Thick Plate," Materials Science and Engineering: A, 478, (2008), 351-360.

7. ARL report number ARL-TR-5212

8. J. B. Sha, J. Sun, Z. J. Deng, and H. J. Zhou, "Micro-Crack Tip Fracture of Commercial Grade Aluminum Under Mixed Mode Loading," *Theoretical and Applied Fracture Mechanics*, 31 (1999), 119-130.